Journal of Microscopy, Vol. 218, Pt 2 May 2005, pp. 148–159
Received 16 November 2004; accepted 27 February 2005

Performance comparison between the high-speed Yokogawa spinning disc confocal system and single-point scanning confocal systems

E. WANG, C. M. BABBEY & K. W. DUNN
Department of Medicine, Division of Nephrology, Indiana University Medical Center, Indianapolis, IN 46202–5116, U.S.A.

Key words. Photobleaching, single-point scanning confocal, spinning disc confocal.

Summary

Fluorescence microscopy of the dynamics of living cells presents a special challenge to a microscope imaging system, simultaneously requiring both high spatial resolution and high temporal resolution, but with illumination levels low enough to prevent fluorophore damage and cytotoxicity. We have compared the high-speed Yokogawa CSU10 spinning disc confocal system with several conventional single-point scanning confocal (SPSC) microscopes, using the relationship between image signal-to-noise ratio and fluorophore photobleaching as an index of system efficiency. These studies demonstrate that the efficiency of the CSU10 consistently exceeds that of the SPSC systems. The high efficiency of the CSU10 means that quality images can be collected with much lower levels of illumination; the CSU10 was capable of achieving the maximum signal-to-noise of an SPSC system at illumination levels that incur only at 1/15th of the rate of the photobleaching of the SPSC system. Although some of the relative efficiency of the CSU10 system may be attributed to the use of a CCD rather than a photomultiplier detector system, our analyses indicate that high-speed imaging with the SPSC system is limited by fluorescence saturation at the high levels of illumination frequently needed to collect images at high frame rates. The high speed, high efficiency and freedom from fluorescence saturation combine to make the CSU10 effective for extended imaging of living cells at rates capable of capturing the three-dimensional motion of endosomes moving up to several micrometres per second.

Introduction

The development of genetically engineered fluorescent proteins has resulted in a renaissance in fluorescence microscopy of living cells and tissues. Studies of the dynamics of fluorescently tagged molecules have emphasized the need for high-resolution imaging systems capable of collecting images rapidly, but with illumination levels low enough to avoid damaging light-sensitive fluorophores and cells. The difficulty of imaging cellular dynamics is further exaggerated in studies of thick cells and tissues, which require that multiple focal planes be collected for each time point, incurring proportional increases in photobleaching, and decreases in temporal resolution. Thus three-dimensional (3D) imaging over time places the strictest requirements on an imaging system, simultaneously requiring high lateral and axial resolution, high speed and efficiency sufficient to provide usable images with minimal illumination.

Three-dimensional imaging is typically conducted using confocal microscopy based upon a single-point scanning confocal (SPSC) design in which a point of laser illumination is rapidly raster-scanned across a sample, sequentially building up a 2D image as the emissions are simultaneously collected through a confocal pinhole. In most systems this scanning process is slow, with images collected at around one frame per second, a rate too slow to capture dynamics in a 3D volume consisting of 15–30 optical sections. High-speed scanning systems are capable of increasing frame rates of SPSC systems to 30 frames per second (Tsien & Bacskai, 1995), but the rate of image acquisition by SPSC systems is ultimately limited by the number of photons of fluorescence that can be collected from a diffraction-limited area in pixel dwell times lasting fractions of a microsecond. Fluorescence may be increased with more illumination, but only to an upper limit defined by fluorescence saturation, a condition in which the excitation photon flux is high enough to deplete the electronic ground state of the fluorophore, effectively decreasing the amount of 'excitable' fluorophore in the volume.

One way of rapidly collecting confocal images without fluorescence saturation is to parallelize confocal image collection.

Correspondence to: Dr Kenneth W. Dunn. Tel.: +1 317 278 0436; fax: +1 317 274 8575; e-mail: kwdunn@iupui.edu

By collecting a number of points simultaneously, high frame capture rates can be obtained without resorting to very brief, very intense illuminations. For example, much higher frame capture rates can be attained by scanning a line across a sample and collecting fluorescence through a confocal slit. With small image sizes, line-scanning systems are capable of collecting images at hundreds of frames per second. However, these systems offer poorer axial resolution and background rejection (Amos & White, 1995).

Confocal imaging can also be conducted by simultaneously scanning an array of diffraction-limited points across a sample, and collecting fluorescence emissions through a set of confocal pinholes. Generally this approach has been implemented by illuminating a spinning, perforated disc (Nipkow disc) that rotates rapidly enough that the points of fluorescence effectively merge into a 2D image that can be collected with a CCD. The first versions of this design suffered from the poor transmission of illumination through the disc; however, this problem has been alleviated by a recent design that utilizes microlenses to focus 40% of the illuminating light through the pinholes (Tanaami *et al.*, 2002). This system, the Yokogawa CSU10, has found wide utility among cell biologists (Inoue & Inoue, 2002; Nakano, 2002; Adams *et al.*, 2003; Maddox *et al.*, 2003).

Some investigators have noted that extended imaging studies using the CSU10 system are remarkably free of photobleaching and have suggested that its superior performance results from the high efficiency of its CCD detector or from the low illumination dosage of a spinning disc system (Inoue & Inoue, 2002; Maddox *et al.*, 2003). We have applied an assay of the photon economy of a confocal microscope system, as measured by the image signal-to-noise ratio (SNR) returned for a given level of photobleaching, to compare quantitatively the efficiency of the Yokogawa system against several SPSC microscope systems. These studies demonstrate that, when imaging at moderately high rates, the CSU10 system is capable of reproducing the highest SNR measured for an SPSC system at approximately 1/15th of the rate of the photobleaching. At higher levels of illumination, the Yokogawa system is capable of collecting images with SNRs four-fold higher than the highest observed with the SPSC systems. Our analyses also demonstrate significant fluorescence saturation in the SPSC system, but not in the CSU10 system. These observations support the hypothesis that the high-speed performance advantage of the CSU10 at least partially derives from the low photon dosage of its illumination system, which limits peak illumination to a small fraction of that of the SPSC systems. Thus the superior performance of the CSU10 results not only from a more efficient mechanism of fluorescence collection, but also a more efficient mechanism of fluorescence excitation. These characteristics, together with the high frame rate of the system, combine to make the CSU10 particularly effective for 4D imaging of living cells.

Methods and materials

Microscope systems

The Yokogawa CSU10 spinning disc confocal scanner system was evaluated using a Perkin-Elmer Ultraview system mounted on a Nikon TE 2000U inverted microscope, using Nikon 60× or 100× NA 1.4, oil-immersion planapochromatic objectives. The system is equipped with a Hamamatsu Orca-ER CCD system (Bridgewater, NJ, U.S.A.). Comparison studies were conducted on several SPSC systems, including a Bio-Rad MRC-1024 confocal scanner mounted on a Nikon Eclipse 200 inverted microscope, using the same Nikon 100× or 60× NA 1.4 oil-immersion objectives, a Zeiss LSM-510 confocal scanner attached to a Zeiss Axiovert 100M inverted microscope, a Zeiss LSM-510-META confocal scanner mounted on a Zeiss Axioplan upright microscope using a Zeiss 100×, NA 1.4 oil-immersion planapochromatic objective and an Olympus FV1000 system, using a 60×, NA 1.4 oil-immersion objective.

Live cell microscopy

Fluorescence studies were conducted using the PTR clone of strain II cells, transfected with both the human transferrin receptor (TfR) and the rabbit polymeric immunoglobulin receptor (pIgR) or with Madin-Darby Canine Kidney (MDCK) strain II cells stably transfected with both rabbit pIgR and green fluorescent protein (GFP)-Rab25 (Wang *et al.*, 2001). Endosomes were labelled by incubation in 20 μg mL^{-1} TexasRed-transferrin in Medium 1 (150 mM NaCl, 20 mM HEPES, 1 mM $CaCl_2$, 5 mM KCl, 1 mM $MgCl_2$, 10 mM glucose, pH 7.4) on the microscope stage maintained at 37 °C with a microscope stage heater, using either a Warner Instruments TC324B (Hamden, CT, U.S.A.) or Medical Systems Corp. PDMI-2 (Greenvale, NY, U.S.A.). TexasRed-transferrin was prepared from the succinimidyl ester of Texas Red, obtained from Molecular Probes (Eugene, OR, U.S.A.), as described previously (Wang *et al.*, 2001).

Measurements of resolution

Subresolution fluorescent beads, 0.1 μm (Molecular Probes), were diluted in 0.1 mg mL^{-1} poly-D-lysine solution. A dilute solution of beads was spread evenly on a cover slip, air-dried at room temperature and mounted in ~5 μL glycerol. SPSC images were Kalman averaged for four frames, and images from the CSU10 were integrated for 300 ms. Vertical stacks of images were collected on both systems at an interval of 0.1 μm, with a pixel size of 0.067 μm for 100× objectives, and 0.112 μm for the 60× objective.

Measurements of SNR and photobleaching rates

InSpeck Green (505/515) Microscope Image Intensity Calibration Kit, 2.5-μm fluorescent beads (Molecular Probes) were

spread evenly onto cover slips. The spread beads suspension was air-dried at room temperature and the cover slip was then placed on top of an 8-μL glycerol droplet on a slide.

Images were collected with acquisition settings as comparable as possible for the CSU10 and SPSC systems. In both cases, 100× NA 1.4 planapochromatic objectives were used. The same pixel size was achieved by adjusting the zoom of the SPSC system to yield 0.067-μm pixels, the fixed pixel size of the CSU10 with a 100× objective (measured with a stage micrometer). The pinhole was set to 1 Airy unit on the SPSC system to match the CSU10 system. For both systems, 512 × 512-pixel, 12-bit images were collected at 1.66 frames per second, the maximum speed of the SPSC system for this frame/pixel size. For both systems, illumination was provided by the 488-nm line of an Ar laser, and the same type of emission filter (500–550 nm) was used.

The camera gain of the Orca-ER CCD of the CSU10 system was set at minimum, and images were collected without binning, integrated for 573 ms, at a readout rate of 14.75 MHz pixel^{-1}. The photomultiplier tube voltage of the SPSC systems was set within the range in which image SNRs were found to be constant and maximal. As SNRs were found to be independent of camera gain of the CCD on the CSU10 and independent of PMT gain on the SPSC systems, the SNR performance of each system was determined only by illumination level and system design. A series of 100 images was collected for each over a range of illumination levels. Throughout the collection, detector saturation was avoided.

SNR and photobleaching measurements were made using Metamorph software (Universal Imaging, Downington, PA, U.S.A.) and a custom-written program, following a procedure developed by Murray (1998). For measurements of signal, the original image is first smoothed using a 3 × 3 low-pass filter. A threshold was determined to create a bead mask and signal was measured from the mean intensity of pixels within the mask, after subtracting the background.

The conventional method for estimating image noise is based upon the variation of pixel intensities around a mean in a homogeneous field. As the design of our studies required imaging a heterogeneous sample of fluorescent beads, we used the equivalent procedure in which noise is estimated from the variation around a local mean, as defined by a 3 × 3 mean filter. In this calculation the 3 × 3 mean filtered image provides the local mean value for each pixel. The departure of each pixel from this local mean reflects pixel noise. A 'noise image' is created by subtracting the local mean value from the original value for each pixel in the image. The intensity of each pixel in the noise image is then squared, and noise estimated as the square root of the sum of these squared values (root mean square). This noise estimate is based upon the assumption that intensity variations on the scale of single pixels are determined by noise, a reasonable assumption as the 0.067-μm pixel size is small relative to the resolution of the system. In separate measurements of homogeneous samples, this method yielded noise estimates similar to those in which noise is measured from field-wise spatial variability.

Photobleaching rates were obtained by fitting the single exponential curve to the signal values of the first 20 images in each time series. The SNR value for the bead prior to photobleaching was obtained by extrapolating the exponential curve back to the 0th exposure point.

Our approach to measuring system SNR follows that of Murray (1998), with one exception. In order to incorporate image resolution into the system efficiency measurement, Murray analysed SNR in subresolution sized fluorescent beads. We analysed images of 2.5-μm beads, which we found provided more consistent measurements, and separately verified that the resolution of the two systems was similar.

Calculations of pixel dwell times and peak illumination intensities

Our calculations of instantaneous illumination levels are based upon the following calculations. The disc of the CSU10 is perforated with 12 sets of pinholes arranged in a constant pitch helical pattern so that when the disc is rotated at 30 revolutions per second, a given point in the sample is illuminated 360 times per second. Because only 4% of the disc is perforated (Inoue & Inoue, 2002; Maddox *et al.*, 2003), this point actually spends 96% of the time between illuminations. Thus, in the case of an image collected for 1 s, the point is illuminated for a total of 40 ms. As there are 360 illuminations per second, the duration of each illumination is 40/360 or 111 μs. In contrast to the CSU10 system, the pixel dwell time in an SPSC system is varied to achieve a particular frame rate. For the signal-to-noise studies described here, images were collected at a rate of one every 590 ms. At this rate, the pixel dwell time of the SPSC system was 0.96 μs, or 116 times shorter than that for the CSU10. In the course of collecting a single image, each pixel was illuminated once for the SPSC system, whereas each pixel was illuminated 212 times (0.59 × 360) for the CSU10 system. Thus, for this frame rate and pixel dwell time of the SPSC, the instantaneous illumination level is 212 × 116, or 24 592-fold higher on the SPSC for an equivalent total illumination.

Illumination power measurements were made in triplicate measurements at the back aperture of the objective, using a 13PDC001 power meter and 113PDH003 integrating sphere from Melles Griot (Carlsbad, CA, U.S.A.).

Image processing for presentation

The images shown here were contrast stretched to enhance the visibility of dim structures using Photoshop (Adobe, Mountain View, CA, U.S.A.). Specific care was taken never to enhance the contrast in such a way that dim objects were deleted from an image. Images to be compared were always processed identically.

Volume renderings were conducted using Voxx, a PC-based image analysis program developed at the Indiana Center for Biological Microscopy (Clendenon *et al.*, 2002) and available free from http://nephrology.iupui.edu/imaging/voxx.

Results

Resolution

We first verified the resolution of our confocal microscopes by collecting image volumes of subresolution fluorescent microspheres. As the pinholes of the CSU10 system are sized to approximately 1 Airy diameter for a 100× NA 1.4 objective lens at 500 nm (according to the manufacturer's specifications), the pinhole of the SPSC system was adjusted to a diameter of 1 Airy unit, and images were collected using the same 100× objective lens. The two systems showed nearly identical horizontal resolution (the full-width of half-maximal profile intensity was 0.21 μm for the SPSC vs. 0.23 μm for the CSU10, Fig. 1A), while the CSU10 system provided somewhat worse axial resolution, with a half-maximal intensity extending 0.71 μm vs. 0.60 μm for the SPSC system (Fig. 1B). We can detect no differences between the two systems in the tails of these profiles, which decline together to background levels with distance from the bead.

Because the size of the pinholes is fixed in the CSU10 system, resolution is necessarily worse when using lower power objectives for which the pinholes are oversized. As expected, when images were collected with a 60× NA 1.4 objective, the axial resolution of the CSU10 system decreased, with half-maximal intensity approaching 0.85 μm (Fig. 1C). In contrast, when the size of the adjustable pinhole of the SPSC system was reduced to accommodate the smaller Airy disc of the 60× objective, the system provided axial resolution of 0.52 μm.

High-speed confocal microscopy

Because the spinning disc of the CSU10 scans the field 360 times per second, the system has the potential to collect images at very high rates. In practice, the rate of image acquisition is limited by both the pixel clock rate of the CCD and the amount of available signal. The 14.75-MHz bandwidth of the system used here limits image transfer rates to nine full frames (1344 × 1024 pixels) per second, or 23 frames per second when the image size is reduced to 256 × 256. These are theoretical upper limits, as they do not include time to integrate the fluorescent signal. Although image capture rates will obviously slow as integration times increase to accommodate weak signals, actual image capture rates can approach these values because image integration can occur simultaneously with data transfer in the interline-transfer CCD used here.

For example, in many of our samples, adequate signal is obtained with integrations of 36 ms, allowing us to collect 256 × 256-pixel images at 20 frames per second. An example is shown in Fig. 2(A), which shows the first of 600 images of living MDCK cells expressing a chimera of GFP and the vesicle-associated protein Rab25. Two versions of this time series may be viewed as movies at http://www.nephrology.iupui.edu/wang_etal. The first, Movie 2A-actual, shows the first 200 frames of the time series, displayed at the same rate at which the images were collected (20 frames per second). The second, Movie 2A-3X, shows the entire 600-frame time series displayed at 3× the actual rate. The first animation demonstrates the actual speed with which the Rab25-associated endosomes move through the cells in the field. The second animation emphasizes the activity, but is more noteworthy for the fact that the fluorescence of the endosomes is largely undiminished. Quantifications of images at the beginning and end of the time series

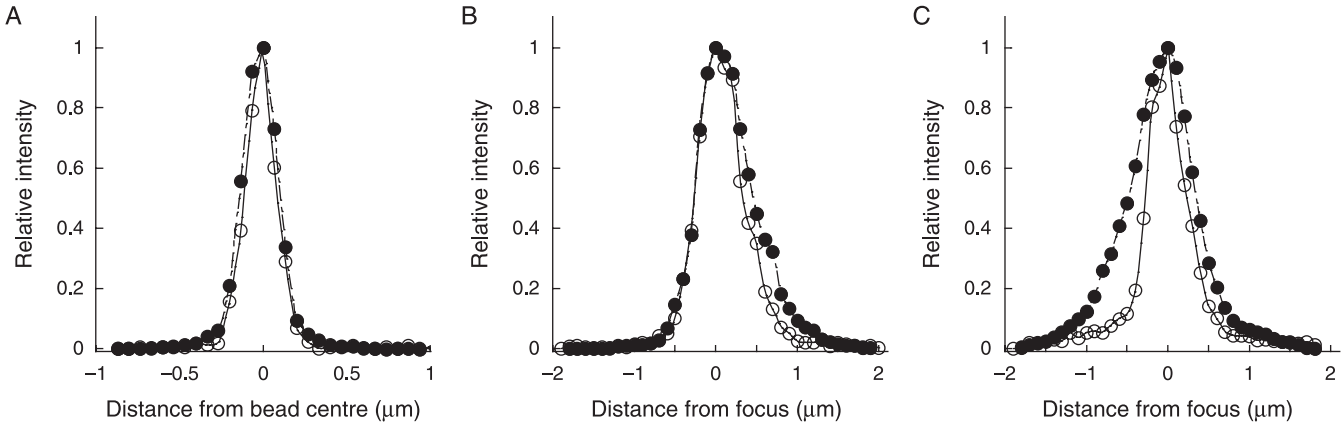

Fig. 1. Comparison of the resolution of the CSU10 system and a conventional single-point-scanning system. (A) Horizontal resolution of the CSU10 (closed circles) and conventional SPSC (open circles) systems. For each system a stack of images of 0.1-μm-diameter fluorescent beads were collected with an axial spacing of 0.1 μm and a pixel width of 0.067 μm using the same 100×, NA 1.4 Planapo oil-immersion objective. (B) Axial resolution of the CSU10 (closed circles) and conventional SPSC (open circles) systems. (C) Axial resolution of the CSU10 (closed circles) and conventional SPSC (open circles) systems using the same 60×, NA 1.4 oil-immersion objective.

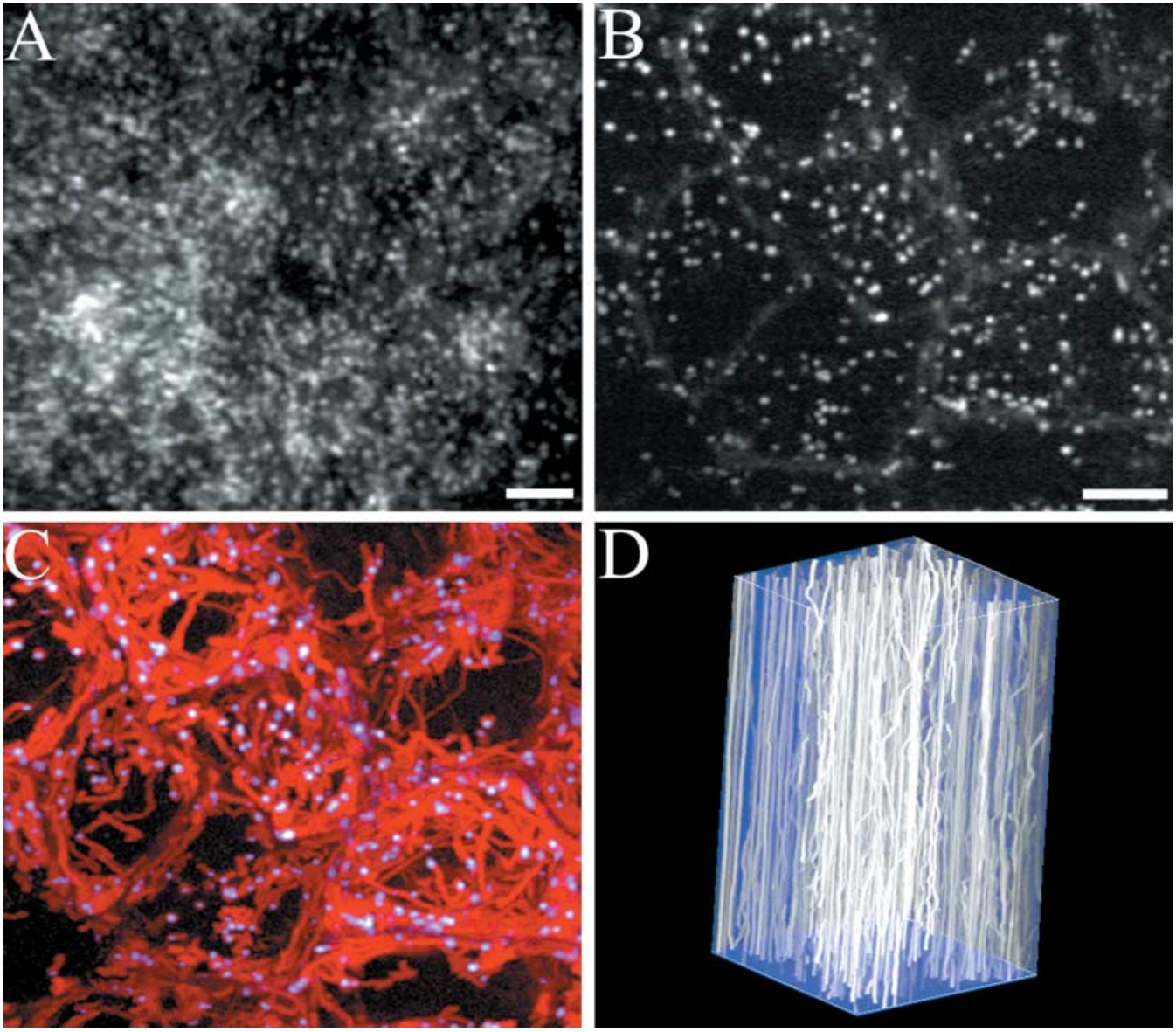

Fig. 2. High-speed imaging of endosomes in living MDCK cells. (A) The first frame of a time series of images of a field of cells expressing GFP-Rab25, a vesicle-associated protein, collected at 20 frames per second over a period of 30 s. Animations of this time series may be found at www.nephrology.iupui.edu/wang_etal. The entire time series is replayed at 3× its actual rate in Movie 2A-3X, and Movie 2A-actual shows an abbreviated time series played at the actual rate. 252 × 256-pixel images, binned 2 × 2, were collected with a 60×, NA 1.2 water-immersion objective. (B) The first frame of a time series of images of a field of cells incubating in a solution of TexasRed-labelled transferrin, a protein that is internalized into endosomes, collected at 11 frames per second over a period of 100 s. The entire time series is replayed at 3× its actual rate in Movie 2B-3X, whereas the Movie 2B-actual shows an abbreviated time series played at the actual rate. This time series is summarized in C, where the original endosome positions are shown in blue, and the subsequent trajectories in the image plane shown in red. D presents another summary of the endosome trajectories of B and C in a 3D volume in which the vertical axis represents time. Different perspectives of this volume can be viewed on the accompanying animation (Movie 2D). 256 × 224-pixel images, binned 2 × 2, were collected with a 100×, NA 1.4 oil-immersion objective. Scale bars = 5 μm.

demonstrate that fluorescence is decreased by only 7% over the collection of 600 images.

The first image of a similar time series is shown in Fig. 2(B), which shows a field of living MDCK cells incubating in a medium containing TexasRed-labelled transferrin, a protein that is internalized into endosomes. The optical sectioning of the system is such that bright images of endosomes are obtained, and the background fluorescence of transferrin in the medium is suppressed. Two versions of this time series are presented at the website. The first, Movie 2B-actual, is replayed at its true rate, 11 frames per second, whereas in the second, Movie 2B-3X, the entire 1110-frame time series is displayed at 3× the

actual speed. The motion of the endosomes is summarized in Fig. 2(C), in which the original endosome positions are displayed in blue, and the trajectories of the endosomes over the 100-s period of imaging are shown in red. As in the field shown in Fig. 2(A), this time series is noteworthy for the minimal effect of protracted illumination on endosome fluorescence. In fact quantifications of endosome fluorescence show a small increase (2%), a result that may reflect the continuous turnover of fluorescent transferrin in the endosomes. The relatively constant endosome fluorescence is more apparent in Fig. 2(D) (and its accompanying animation, Movie 2D), in which the entire time series is displayed as a 3D volume, with the vertical axis representing time (an *xyt* volume). The lack of photobleaching in the field is apparent from the constant intensity of the individual endosome traces.

Photobleaching and sensitivity analyses

The time series shown in Fig. 2 indicate that the CSU10 system is capable of extended image collection with minimal damage to the cells or to the fluorophore. We compared the performance of the CSU10 system with an SPSC system, by collecting time series of fluorescence images of GFP-Rab25 in transfected MDCK cells. A series of 200 images were collected at 2 frames per second (the highest speed at which the SPSC system could collect 256×256-pixel images with sufficient signal) using 100× NA 1.4 oil-immersion objectives. Figure 3(A,B) show the first and last frames, respectively, collected with the CSU10 system, and Fig. 3(D,E) show the first and last frames, respectively, collected with the SPSC system. Whereas the level of endosome fluorescence is relatively unaffected by repeated imaging by the CSU10 system, the endosomes are essentially

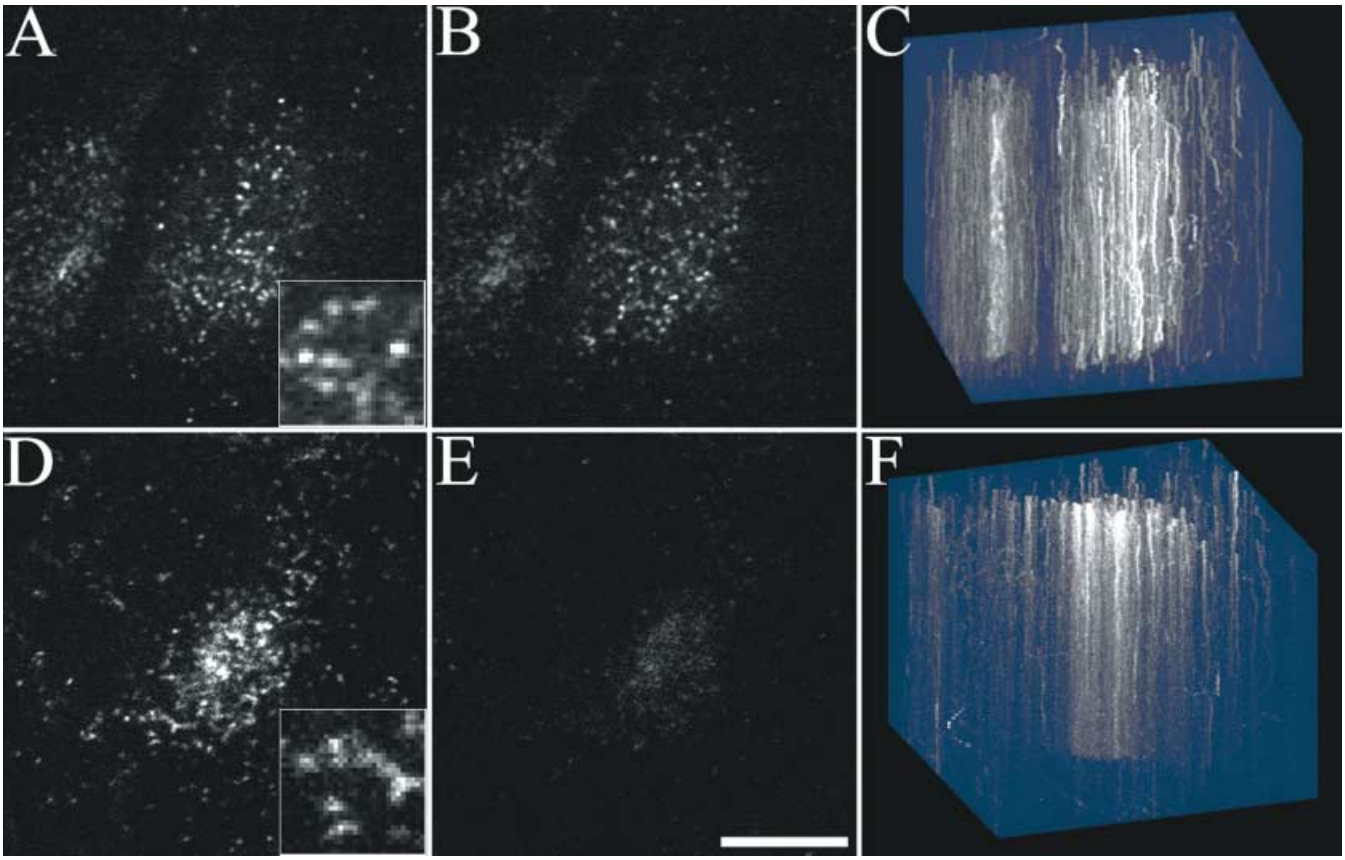

Fig. 3. High-speed time series imaging of MDCK cells stably expressing GFP-Rab25; comparison of the CSU10 spinning disc system with a conventional SPSC system. (A) The first of a time series of images collected with the CSU10; (B) the 200th image. Comparison of the two panels reveals minimal photobleaching over the interval, an impression more directly demonstrated in C (and its accompanying animation, Movie C), which represents the time series of images as a volume in which time is represented as the vertical axis. (D–F) The corresponding images collected with a conventional single-point-scanning system. Comparison of D and E, and inspection of F (and its accompanying animation, Movie 3F) shows that the intensity of the endosome fluorescence is obviously diminished by the 200th image collected with this system. Animations of the time series (Movies 3A and D) are shown at 8× their actual rates. For both systems, images were collected at 2 frames per second, with a pixel size of 0.13 μm, and a frame size of 256×256 pixels, using a 100×, NA 1.4 Planapo oil-immersion objective, with the confocal pinholes set at 1 Airy diameter. Scale bar = 10 μm. Insets, showing magnified portions of A and D, are 4 μm across.

invisible by the end of the time series collected with the SPSC system. The difference in photobleaching between the two systems is also apparent in the animations of the time series (Movies 3A and D), or in the *xyt* image volumes shown in Fig. 3(C,F) (and their accompanying animations, Movies 3C and F).

The comparison shown in Fig. 3 is compelling but not rigorous. Although images were collected with comparable settings as far as possible (with the same pinhole size, pixel size and frame rate), it is possible that this test underestimated the performance of the SPSC system by utilizing too high a level of illumination. Although this is unlikely, given that the highmagnification insets shown in Fig. 3(A,D) suggest better signal-to-noise in the CSU10 image, we next conducted a more rigorous comparison of the two systems, following a modified version of the protocol described by Murray (1998) (see Methods).

In this analysis, the efficiency of a microscope system can be evaluated from the signal-to-noise of its images attained from a given level of illumination, as estimated from the rate of fluorescence photobleaching. Time series of images of fluorescent microspheres were collected at various levels of illumination using either the CSU10 or an SPSC system set with comparable imaging parameters as much as possible (see Methods), with each system collecting 1.66 images per second. For each bead image, signal was estimated from the mean pixel fluorescence in a threshholded region, and noise was measured as the root mean square deviation of the individual pixel intensities from a 3×3 low-pass filter.

The results of these studies are summarized in Fig. 4. Figure 4(A,B) each show horizontal intensity profiles through one particular bead initially and after collection of 100 frames at the highest levels of illumination for the SPSC and CSU10, respectively. Filled circles show the region of the bead used to quantify the total summed fluorescence of the bead, and the 3×3 low-pass filtered images are shown as solid lines. In both figures the pixel values of the original image fluctuate around the values of its smoothed version. However, the fluctuation with the SPSC system is substantially more than with the CSU10.

The mean pixel fluorescence of approximately 30 beads was quantified for each point in the time series for each level of illumination, resulting in a set of photobleaching curves for the two systems (Fig. 4C,D). Photobleach decay rates were measured from a single exponential decay curve fit to the first 20 time points of each time series and plotted against the original SNR, as estimated by extrapolating the SNR curve back to the 0th exposure point (Fig. 4E). This analysis demonstrates that although the two systems have similar SNR values at extremely low illumination levels, with increasing illumination the SNR of the CSU10 system increases much more rapidly than the SPSC system, such that at the highest levels of illumination the SNR of the CSU10 is more than four times that of the SPSC system.

It should be emphasized that the SPSC system used for this analysis had a theoretical advantage over the CSU10 as it was attached to an upright microscope stand, whose more direct lightpath to the detector should be more efficient than that of the inverted stand-mounted CSU10 system. Consistent with this, slightly worse performance was measured in an otherwise identical SPSC system mounted on an inverted microscope stand (with a maximum SNR of 17). Similar tests were performed with SPSC systems from two other manufacturers, but neither performed better than the SPSC system characterized in Fig. 4. Thus the SNR performance of the CSU10 was significantly better than that of four different SPSC systems from three different manufacturers.

The role of fluorescence saturation in high-speed confocal microscopy

Some of the performance disparity between the systems evaluated here may result from the higher quantum efficiency of the ORCA-ER CCD of the CSU10 as compared with PMT detectors of the SPSC systems evaluated here. However, quantum efficiency of the CCD system would have to be 16 times that of the PMT systems to explain the four-fold difference in signal-to-noise performance. In addition, our data suggest that the performance of the SPSC system is not determined simply by the sensitivity and noise characteristics of its detector system. For shot-noise-limited imaging, such as that here, signal-to-noise should increase as the square root of signal. Although this is true for the CSU10, it is true only at the lowest levels of illumination for the SPSC system, suggesting additional limiting factors.

The bulk of the difference in performance may result from the difference in how the two systems collect fluorescence

Fig. 4. Comparison of the efficiency of the CSU10 system and a conventional single-point-scanning system. For both systems a series of images of 2.5-μm-diameter fluorescent beads were collected at 1.66 frames per second with a pixel size of 0.067 μm, and a frame size of 512×512 pixels, using a 100×, NA 1.4 Planapo oil-immersion objective. For the conventional SPSC system, the confocal pinhole was set at 1 Airy diameter and PMT voltage was set in the range where image SNR is independent of voltage. (A) Representative intensity profiles across the image of a bead after the first and 100th frames, collected with the single-point-scanning system. (C) Decay of the mean fluorescence of fields of fluorescent beads (each containing approximately 30 beads) imaged at varying levels of illumination over the course of 100 frames. The corresponding data collected with the CSU10 system are shown in B and D. For each bead a mean signal was calculated from the mean intensity of a masked region of the bead (filled circles), a root-mean-squared noise was calculated from the deviations of the detected pixel intensities from the corresponding values after applying a 3×3 mean smoothing filter (solid lines), and a photobleaching rate was determined from a single-exponential fit to the first 20 points of the fluorescence decay curve. The results of this analysis are presented in E, which shows the relationship between image SNR and photobleaching rate for the CSU10 (squares) and the conventional SPSC system (triangles).

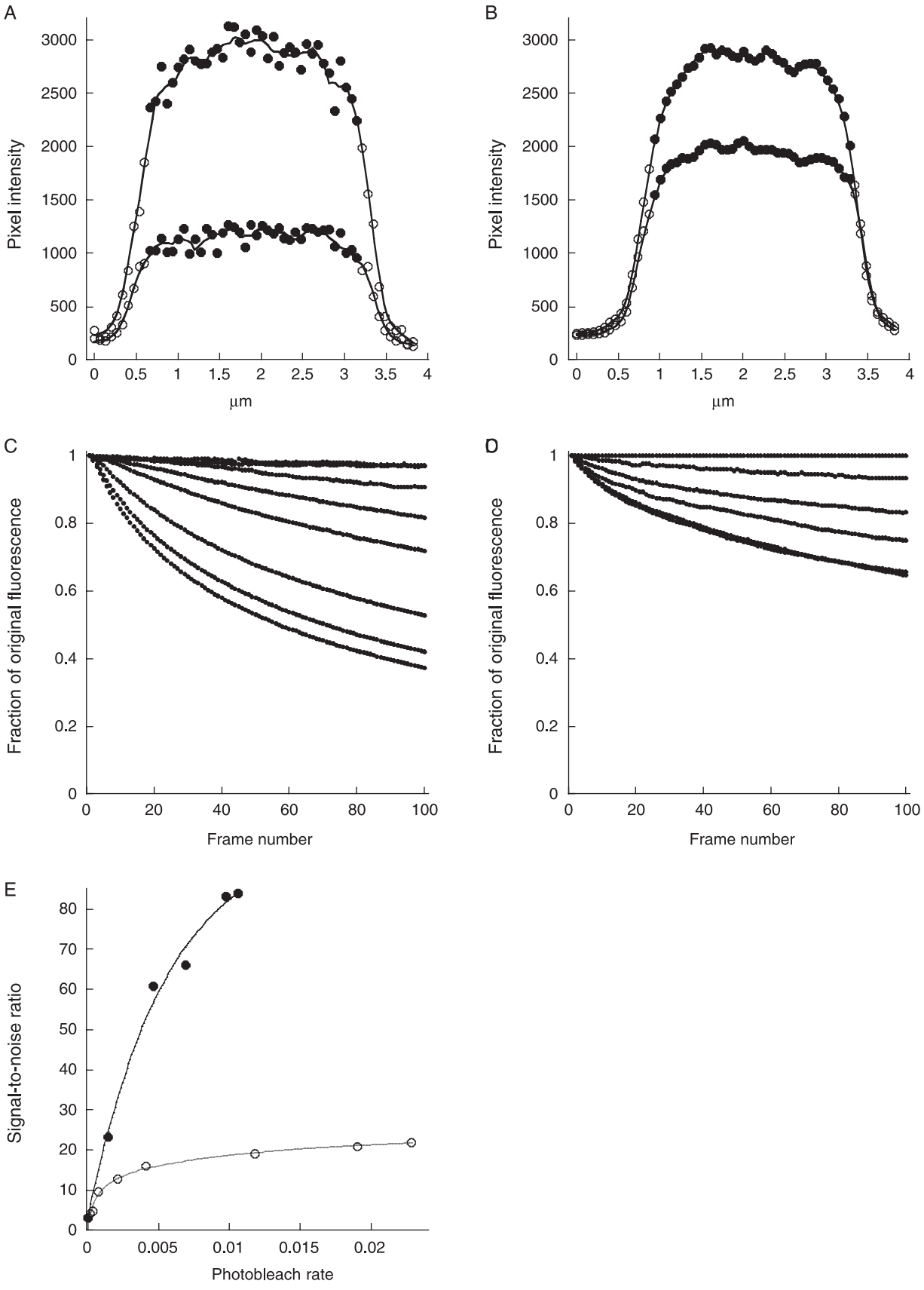
A
Pixel intensity
3000
2500
2000
1500
1000
500
0
0 0.5 1 1.5 2 2.5 3 3.5 4
μm
B
Pixel intensity
3000
2500
2000
1500
1000
500
0
0 0.5 1 1.5 2 2.5 3 3.5 4
μm
C
Fraction of original fluorescence
1
0.8
0.6
0.4
0.2
0
0 20 40 60 80 100
Frame number
D
Fraction of original fluorescence
1
0.8
0.6
0.4
0.2
0
0 20 40 60 80 100
Frame number
E
Signal-to-noise ratio
80
70
60
50
40
30
20
10
0
0 0.005 0.01 0.015 0.02
Photobleach rate

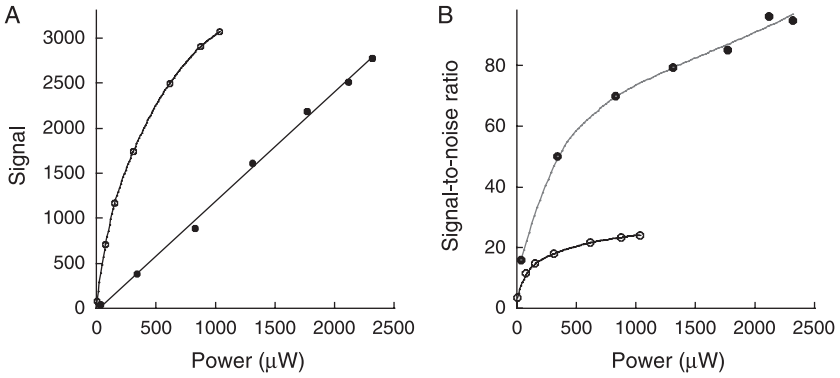

Fig. 5. Fluorescence saturation in SPSC, but not CSU10 systems. (A) The relationship between signal and illumination power for the CSU10 (solid circles) and the SPSC system (open circles) when imaging at 1.66 frames per second. Whereas signal increased linearly with power for the CSU10, the SPSC system clearly saturates at high power levels. (B) Relationship between SNR and illumination power for the CSU10 (closed circles) and the SPSC systems (open circles). Smooth curves were fit by hand.

images, specifically from the greater susceptibility of the SPSC system to fluorescence saturation (Inoue & Inoue, 2002; Maddox *et al.*, 2003). The high-speed performance of SPSC systems is limited by the fact that in order to collect sufficient fluorescence in pixel dwell times lasting only microseconds (0.96 μs in the case shown here), SPSC systems will frequently need to be operated with very high levels of illumination, levels that can be sufficient to saturate fluorophore fluorescence (Sandison *et al.*, 1995; Sheppard *et al.*, 1995). In contrast, the illumination of the CSU10 system is spread over a large number of relatively long illuminations. For the specific case shown here, illumination is spread over 212 doses, each lasting 116 times as long as the single illumination of the SPSC system. In this case, for the same total integrated illumination, the peak illumination of the Yokogawa system is less than 1/24 000th that of the SPSC system.

Fluorescence saturation can be detected as a departure from a linear relationship between fluorescence and illumination power. In order to evaluate the significance of fluorescence saturation in the performance of the SPSC system, we repeated the studies described above, measuring bead signal levels and illumination power over the same range of illumination levels. As shown in Fig. 5(A), we found that whereas fluorescence increases linearly with power for the CSU10 system, the rate of fluorescence excitation clearly slows with increasing power in the SPSC system. Note that although it appears in this plot as if the SPSC is returning a higher signal for a given power level, these values are compensated for by higher noise levels, as in the previous analysis. The resulting relationships between SNR and illumination (Fig. 5B) are nearly identical to those of SNR and photobleaching rate shown in Fig. 4. These results indicate that the performance of the SPSC is at least partially limited by fluorescence saturation when imaging at moderately high frame rates.

Four-dimensional microscopy with the CSU10 – 3D imaging over time

The combined speed and efficiency of the CSU10 makes it uniquely suitable for collecting 3D image volumes over time. The system not only collects images rapidly enough to follow individual endosomes in three dimensions, but also collects high-quality images even after the hundreds or thousands of illuminations needed for 3D imaging over time.

Figure 6(A) shows a stereo anaglyph of the first of 49 image volumes collected from a 9-μm-high field of cells incubating in fluorescent transferrin. This time series was captured at 9 frames per second, or one 18-section volume every 2 s. Despite the relatively coarse temporal sampling (one volume every 2 s), the individual endosome motions are clear in the animation of the time series (Movie 6A, replayed at 16× actual rate). That this sampling frequency is sufficient is also evidenced in Fig. 6(B), which shows a projection of all of the time points in a single volume, showing the largely unbroken trajectories of the endosomes over the entire 100-s interval of collection.

A similar volume of MDCK cells incubating in fluorescent transferrin is shown in Fig. 6(C), which shows a stereo anaglyph of the first of 113 image volumes collected over 100 s. Brighter labelling in this sample supported an image acquisition rate of 18 frames per second, or slightly more than one 16-plane volume per second. Because of the higher acquisition rate, endosome motion is smoother, as shown in the accompanying animation of the time series (Movie 6C, replayed at 8× actual rate), and in the projected time series (Fig. 6D).

Discussion

The analysis of living cells is a powerful but challenging application of fluorescence microscopy. Fluorescence microscopy is nearly always signal-limited, but the problem is exaggerated in studies of living cells, which severely limit the typical solutions to low SNR. Whereas SNR can be improved by increasing illumination in fixed cells, the level of illumination that may be used for living cells is limited by phototoxicity, and photobleaching of fluorophores. Photobleaching is especially problematic because living cells do not tolerate the chemical singlet oxygen quenchers typically used to reduce photobleaching. Longer image integrations will also improve SNR, but may also render the system incapable of resolving the dynamics that probably motivated the studies in the first place.

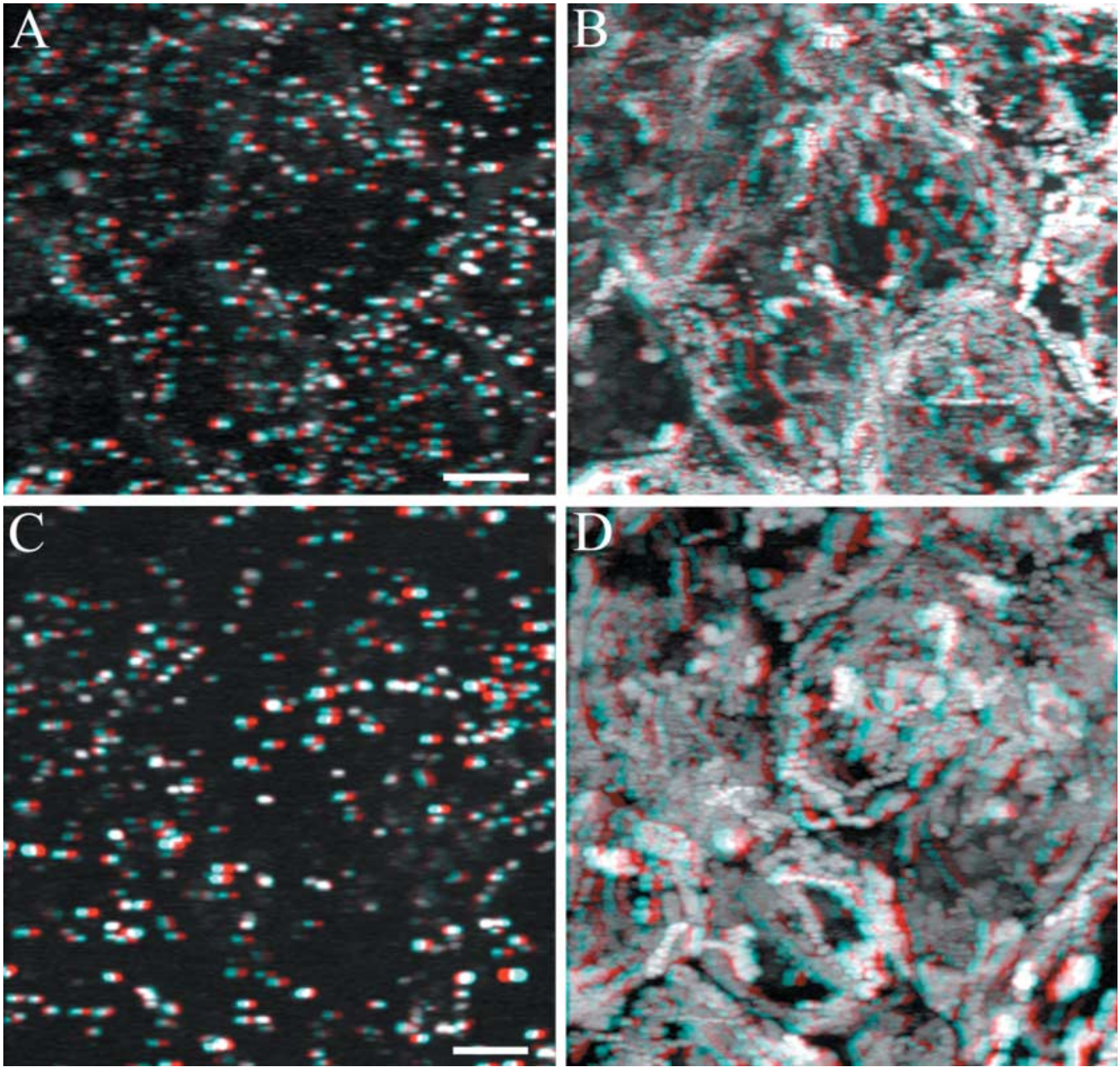

Fig. 6. High-speed 3D imaging of endosomes in living MDCK cells. (A) A stereo anaglyph image of the first volume of a time series of image volumes of a field of cells incubating in a solution of TexasRed-labelled transferrin, collected at 0.5 volumes per second (9 frames per second) over a period of 100 s. For each volume, images were collected every 0.5 μm through a depth of 9 μm. The accompanying animation (Movie 6A) is replayed at 16× its actual rate. 256 × 224-pixel images, binned 2 × 2, were collected with a 100×, NA 1.4 oil-immersion objective. (B) A stereo anaglyph image of the trajectories of the endosomes over the entire interval. (C) A stereo anaglyph image of the first volume of a time series of image volumes of a field of cells incubating in a solution of TexasRed-labelled transferrin, collected at 1.1 volumes per second (18 frames per second) over a period of 100 s. For each volume, images were collected every 0.6 μm through a depth of 9.6 μm. The accompanying animation (Movie 6C) is replayed at 8× its actual rate. (D) A stereo anaglyph image of the trajectories of the endosomes over the entire interval. 256 × 256-pixel images, binned 2 × 2, were collected with a 60×, NA 1.2 water-immersion objective, with a 1.5× magnifying lens. Scale bars = 5 μm.

Numerous studies have demonstrated the capability of the CSU10 system for imaging living cells. Applications include studies of vesicular transport (Nakano, 2002; Kreitzer *et al.*, 2003), actin dynamics (Pelham & Chang, 2002), calcium transients (Ishida *et al.*, 1999), microvascular blood flow (Oyanagi-Tanaka *et al.*, 2001) and microtubule dynamics (Adams *et al.*, 2003; Canman *et al.*, 2003; Hwang *et al.*, 2003).

Some of these investigators have found the CSU10 remarkable for its ability to support extended imaging of living cells with strikingly little photobleaching (Inoue & Inoue, 2002; Maddox *et al.*, 2003). Our studies demonstrate that this relative freedom from photobleaching derives from the high efficiency of the CSU10 system, which supports collection of high-SNR images with very low levels of illumination. The CSU10 is capable of reproducing the highest SNR measured for an SPSC system at approximately 1/15th the rate of photobleaching. At higher levels of illumination the Yokogawa system is capable of collecting images with SNRs four-fold higher than the highest observed with the SPSC systems.

Although the higher efficiency of the CSU10 may partially reflect the inherently better signal-to-noise performance of CCD-based vs. PMT-based detector systems, much of the advantage appears to derive from its freedom from fluorescence saturation. When imaging at moderately high speeds (1.66 frames per second) fluorescence scaled linearly with illumination power for the CSU10, but the rate of fluorescence excitation declined with illumination in the SPSC system. These observations support the hypothesis that the high-speed performance advantage of the CSU10 at least partially derives from the low photon dosage of its illumination system, which limits peak illumination to a small fraction of that of the SPSC systems. Whereas the illumination of the SPSC systems is limited to a single, very brief exposure, the CSU10 system spreads illumination out over a large number of relatively long exposures. When collecting images at 1.66 frames per second, this amounts to 24 000-fold lower peak illumination in the CSU10 system. Thus if illumination levels are increased to compensate for the shorter pixel dwell times necessary for high-speed imaging with SPSC systems, they can rapidly reach levels that saturate fluorescence.

Thus the minimal photobleaching seen in extended studies using the CSU10 system may reflect not only the higher efficiency of CCD-based systems, but also the freedom of this system from the effects of fluorescence saturation, which limits SNRs, decreases resolution, increases background and perhaps accelerates destructive higher order interactions (Sandison *et al.*, 1995). In practice, fluorescence saturation can be detected in a particular study by increasing illumination and evaluating whether signal increases linearly with illumination power.

Collecting signal over multiple illuminations gives the CSU10 additional potential advantages. First, the intervals between illuminations provide fluorophores with multiple opportunities to return to the ground state, effectively increasing the concentration of 'excitable' fluorophore. For each second of image collection, fluorophores are given 360 dark intervals (without illumination), each lasting 2.7 ms. This is more than sufficient time for all electrons in the excited state and most (if not all) of those in the long-lived triplet state to return to the ground state. While, as discussed above, the levels of illumination used for the CSU10 will seldom induce an accumulation of electrons in the excited state, the significance of the triplet state is less clear.

Another advantage of the CSU10 is that, in the course of integrating many observations, noise is effectively averaged, reducing it by $1/\sqrt{n}$. For shot noise, integrating many observations results in a noise estimate that is mathematically equivalent to that for a single observation of the integrated sum. However, multiple sampling can statistically reduce other sources of noise such as that resulting from laser power fluctuations. For example, the power output of Ar lasers may vary by 1% or more at megahertz frequencies and thus can substantively contribute to variations between adjacent pixels in SPSC systems (Swedlow *et al.*, 2002).

Although the spinning disc design of the CSU10 has significant advantages over SPSC systems for high-speed imaging, SPSC systems have several advantages over the CSU10, making it more suitable for many applications. First, whereas we have found that the CSU10 provides similar background rejection for thin specimens, it is less successful with thicker samples with significant amounts of out-of-focus fluorescence, for which crosstalk between adjacent pinholes on the disc becomes significant (Reichelt & Amos, 2001; Egner *et al.*, 2002). SPSC systems are also far more flexible. Whereas the size of the confocal apertures of the CSU10 is fixed, limiting truly confocal operation to a 100×, NA 1.4 objective, the pinhole size of SPSC systems can be varied to suit different microscope objectives and different experimental needs. Unlike the CSU10, SPSC systems offer the capability of altering the size of the scanned area. This capability supports flexible sizing of pixels to optimize digital sampling, and is also necessary for studies of the dynamics of photobleaching recovery. Unlike SPSC systems that can simultaneously collect multiple channels in perfect registration, multicolour images must be collected in series with the CSU10 system, or by using optically complex image-splitting systems. Finally, quantitative studies are complicated in the CSU10 by a field of illumination that is less homogeneous than that for SPSC systems, due to the difficulty of homogeneously illuminating the disc with an expanded laser beam.

Thus, depending upon the application, SPSC systems will frequently provide more capabilities than the CSU10. Insofar as the CSU10 is limited to relatively thin samples, wide-field microscopy should likewise be considered as an alternative which would provide the same speed, and would enjoy the same advantages from CCD detection and low photon dosage. A quantitative comparison of confocal and wide-field microscope systems found that wide-field systems are better capable of resolving dim objects, apparently because of their superior noise performance (Swedlow *et al.*, 2002). Optical sectioning equivalent to that found in confocal microscopes can be provided through digital deconvolution (Swedlow & Platani, 2002), which also has the effect of increasing the signal-to-noise of dim objects (Swedlow *et al.*, 2002). However, relatively high levels of fluorescence are needed to make this approach

practical, as image deconvolution is very sensitive to image noise (van Kempen *et al*., 1997; Verveer *et al*., 1999), which invariably accompanies imaging at high speed.

In summary, by implementing a system of microlenses on a spinning disc, Yokogawa has realized the potential of the Nipkow-based confocal microscope system for biological microscopy. Not only is the CSU10 capable of collecting images much more rapidly than SPSC systems, it does so with much higher efficiency. The performance advantage of the CSU10 system derives not only from its more efficient collection, but also from more efficient excitation made possible by an illumination system that maximizes the population of fluorophores in the ground state, effectively optimizing the amount of fluorescence stimulated from a given number of fluorophore molecules. Together, these characteristics support extended 4D imaging of living cells at rates sufficient to capture the 3D motion of intracellular vesicles moving up to several micrometres per second.

Acknowledgements

This research was supported by NIH grants RO1 DK51098 and P50 DK 61594–01 (K.W.D.) and a grant (Indiana Genomics Initiative) from the Lilly Endowment to the Indiana University School of Medicine. The studies were conducted at the Indiana Center for Biological Microscopy.

References

Adams, M.C., Salmon, W.C., Gupton, S.L., Cohan, C.S., Wittmann, T., Prigozhina, N. & Waterman-Storer, C.M. (2003) A high-speed multi-spectral spinning-disk confocal microscope system for fluorescent speckle microscopy of living cells. *Methods*, **29**, 29–41.

Amos, W.B. & White, J.G. (1995) Direct view confocal imaging systems using a slit aperture. *Handbook of Biological Confocal Microscopy* (ed. by J.B. Pawley), pp. 403–415. Plenum, New York.

Canman, J.C., Cameron, L.A., Maddox, P.S., Straight, A., Tirnauer, J.S., Mitchison, T.J., Fang, G., Kapoor, T.M. & Salmon, E.D. (2003) Determining the position of the cell division plane. *Nature*, **424**, 1074–1078.

Clendenon, J.L., Phillips, C.L., Sandoval, R.M., Fang, S. & Dunn, K.W. (2002) Voxx: a PC-based, near real-time volume rendering system for biological microscopy. *Am. J. Physiol. – Cell Physiol.* **282**, C213–C218.

Egner, A., Andresen, V. & Hell, S.W. (2002) Comparison of the axial resolution of practical Nipkow-disk confocal fluorescence microscopy with that of multifocal multiphoton microscopy: theory and experiment. *J. Microsc*. **206**, 1–32.

Hwang, E., Kusch, J., Barral, Y. & Huffaker, T.C. (2003) Spindle orientation in *Saccharomyces cerevisiae* depends on the transport of microtubule ends along polarized actin cables. *J. Cell Biol*. **161**, 483–488.

Inoue, S. & Inoue, T. (2002) Direct-view high-speed confocal scanner: the CSU-10. *Methods Cell Biol*. **70**, 87–127.

Ishida, H., Genka, C., Hirota, Y., Nakazawa, H. & Barry, W.H. (1999) Formation of planar and spiral Ca^{2+} waves in isolated cardiac myocytes. *Biophys. J*. **77**, 2114–2122.

van Kempen, G.M.P., van Vliet, L.J., Verveer, P.J. & van der Voort, H.T.M. (1997) A quantitative comparison of image restoration methods for confocal microscopy. *J. Microsc*. **185**, 354–365.

Kreitzer, G., Schmoranzer, J., Low, S.H., Li, X., Gan, Y., Weimbs, T., Simon, S.M. & Rodriguez-Boulan, E. (2003) Three-dimensional analysis of post-Golgi carrier exocytosis in epithelial cells. *Nature Cell Biol*. **5**, 126–136.

Maddox, P.S., Moree, B., Canman, J.C. & Salmon, E.D. (2003) Spinning disk confocal microscope system for rapid high-resolution, multimode, fluorescence speckle microscopy and green fluorescent protein imaging in living cells. *Methods Enzymol*. **360**, 597–617.

Murray, J.M. (1998) Evaluating the performance of fluorescence microscopes. *J. Microsc*. **191**, 128–134.

Nakano, A. (2002) Spinning-disk confocal microscopy – a cutting-edge tool for imaging of membrane traffic. *Cell Structure Function*, **27**, 349–355.

Oyanagi-Tanaka, Y., Yao, J., Wada, Y., Morioka, T., Suzuki, Y., Gejyo, F., Arakawa, M. & Oite, T. (2001) Real-time observation of hemodynamic changes in glomerular aneurysms induced by anti-Thy-1 antibody. *Kidney Int*. **59**, 252–259.

Pelham, R.J. & Chang, F. (2002) Actin dynamics in the contractile ring during cytokinesis in fission yeast. *Nature*, **419**, 82–86.

Reichelt, S. & Amos, W.B. (2001) SELS: a new method for laser scanning microscopy of live cells. *Microsc. Anal*. **November**, 9–11.

Sandison, D.R., Williams, R.M., Wells, K.S., Strickler, J. & Webb, W.W. (1995) Quantitative Fluorescence confocal laser scanning microscopy (CLSM). *Handbook of Biological Confocal Microscopy* (ed. by J. B. Pawley), pp. 39–53. Plenum, New York.

Sheppard, C.J.R., Gan, X., Gu, M. & Roy, M. (1995) Signal to noise in confocal microscopes. *Handbook of Biological Confocal Microscopy* (ed. by J.B. Pawley), pp. 363–388. Plenum, New York.

Swedlow, J.R., Hu, K., Andrews, P.D., Roos, D.S. & Murray, J.M. (2002) Measuring tubulin content in Toxoplasma gondii: a comparison of laser-scanning confocal and wide-field fluorescence microscopy. *Proc. Natl Acad. Sci. USA*, **99**, 2014–2019.

Swedlow, J.R. & Platani, M. (2002) Live cell imaging using wide-field microscopy and deconvolution. *Cell Structure Function*, **27**, 335–341.

Tanaami, T., Otsuki, S., Tomosada, N., Kosugi, Y., Shimizu, M. & Ishida, H. (2002) High-speed 1-frame/ms scanning confocal microscope with a microlens and Nipkow disks. *Appl. Optics*, **41**, 4704–4708.

Tsien, R.Y. & Bacskai, B. (1995) Video-rate confocal microscopy. *Handbook of Biological Confocal Microscopy* (ed. by J. B. Pawley), pp. 459–478. Plenum, New York.

Verveer, P.J., Gemkow, M.J. & Jovin, T.M. (1999) A comparison of image restoration approaches applied to three-dimensional confocal and wide-field fluorescence microscopy. *J. Microsc*. **193**, 50–61.

Wang, E., Pennington, J.G., Goldenring, J.R., Hunziker, W. & Dunn, K.W. (2001) Brefeldin A rapidly disrupts plasma membrane polarity by blocking polar sorting in common endosomes of MDCK cells. *J. Cell Sci*. **114**, 18–21.